

TURBULENCE TRANSITION IN THE WAKE OF WALL-MOUNTED PRISMS

Shubham Goswami¹, Arman Hemmati²

Department of Mechanical Engineering, University of Alberta, Edmonton, AB, Canada T6G 2R3

¹ goswami@ualberta.ca, ² arman.hemmati@ualberta.ca

Abstract

This article presents a numerical investigation of the turbulence transition phenomenon in the wake of wall-mounted prisms. Large-eddy simulations are performed at $Re = 1 \times 10^3 - 5 \times 10^3$ for prisms at a range of aspect-ratio (0.25 – 1.5) and depth-ratios (1 – 5). The results show that the wake unsteadiness is enhanced with increasing depth-ratio, which is attributed to the interactions between Kelvin-Helmholtz instability of the shear-layer and large-scale vortex shedding. This is driven by the shear-layer flapping motion in the large depth-ratio prism. These interactions elevate the flow momentum due to increased turbulence intensity and mixing, contributing to the wake transition phenomenon. Enhanced interactions are quantified using the Poisson's equation and bi-spectral mode decomposition. This study underscores the role of depth-ratio in the transition phenomenon.

Introduction

The study of separated flows over sharp-edged, wall-mounted bluff bodies, like prisms, has garnered increasing attention due to their relevance in various industrial applications. These flows are notably complex and multifaceted, owing to their inherent three-dimensional nature, which are primarily attributed to end-effects (Wang & Zhou, 2009). As the oncoming flow encounters the leading edge, it decelerates and forms a boundary layer along the prism surfaces. This boundary layer subsequently separates, creating a highly disturbed region of flow known as the wake (Zdravkovich, 1997). One prominent feature of the wake is the formation of large-scale coherent structures, which contain a significant portion of the total fluctuating energy, thus playing a vital role in momentum transfer and mixing processes. The formation of these structures strongly depends on state of the wake, which can be laminar, transitional, or turbulent. Transition can occur in three key regions: (i) within the wake, (ii) in the free-shear layers bordering the wake, and (iii) within the boundary layer. Moreover, transition to turbulence is influenced by both Reynolds number ($Re = U_b d / \nu$, where d is the width of the prism), and geometrical features of the flow. These include the depth-ratio, aspect-ratio ($AR = h/d$, where h is the height of the prism), and free-end effects, particularly in the case of wall-mounted prisms (Zdravkovich, 1997).

At elevated Reynolds numbers ($Re > 10^3$), it is well-documented that separated shear-layers have the capacity to reattach over the side and top surfaces of the prism, provided there is a significant increase in the depth-ratio (Rastan *et al.*, 2021). Further, increasing the depth-ratio entails enhancement of the downwash flow, which suppresses the wake unsteadiness (Goswami & Hemmati, 2022). Meanwhile, the aspect-ratio plays a role in intensifying the upwash flow and con-

tributing to the overall wake unsteadiness (Saha, 2013). Thus, the enhancement of unsteadiness in the wake of wall-mounted prisms can be achieved by either increasing the aspect-ratio or reducing the depth-ratio. This heightened wake unsteadiness suggests that such abrupt changes in geometry may be associated with the transition to turbulence.

Goswami & Hemmati (2022) studied the wake of small aspect-ratio wall-mounted prisms with increasing depth-ratio at low Reynolds numbers and observed the suppression of spatio-temporal features with depth-ratio. Previously, Rastan *et al.* (2021) made similar observations in the low-to-moderate range of Reynolds numbers ($10^3 \leq Re \leq 10^4$). They demonstrated that increasing the depth-ratio led to diminished vortex shedding, which was attributed to the suppressed interactions between the separating shear-layer and the wake. This suppression was linked to the strengthening of the downwash flow. Zargar *et al.* (2022) further demonstrated that increasing the Reynolds number above 750 for a large depth-ratio prism ($DR = 5$) led to an irregular (unstable) unsteady regime resembling a transitional state. The irregular shedding resulted in flow reattachment and subsequent detachment from the prism surfaces. Majority of studies on wall-mounted prisms have focused on low ($10^2 \leq Re \leq 10^3$) and high ($Re \geq 10^4$) Reynolds number ranges, with limited attention given to the moderate range of Reynolds numbers. Since moderate Reynolds numbers ($10^3 \leq Re \leq 10^4$) are associated with the transition to turbulence, it is important to investigate and characterize the wake of wall-mounted prisms in this regime.

The present study investigates the role of depth-ratio in the turbulence transition phenomenon at $10^3 \leq Re \leq 10^4$. Specifically, this study investigates the possibility of enhanced momentum transport with increasing depth-ratio as a precursor to wake transition. We hypothesize that the shear-layer flapping motion enhances the interactions between the leading-edge shear-layer instabilities and prism surfaces, especially at large depth-ratio. This enhanced interaction elevates the flow momentum and contributes to the transition phenomenon. The investigation is performed numerically at Reynolds numbers of $1 \times 10^3 - 5 \times 10^3$ for wall-mounted prisms with aspect-ratios of 0.25 – 1.5 and a range of depth-ratios between 1 – 5. For brevity, only the results at $Re = 2.5 \times 10^3$ are presented for $AR = 1$ and $DR = 1$ and 4.

Computational Setup

Large-eddy Simulations (LES) with the Dynamic Smagorinsky sub-grid scale model (Durbin & Reif, 2011) was utilized to study the wake. The computational domain consisted of a rectangular prism mounted on the base, with the domain extending $34d$ in the streamwise (x) direction, $6d$ in the normal (y) direction, and $12d$ in the spanwise (z) direction.

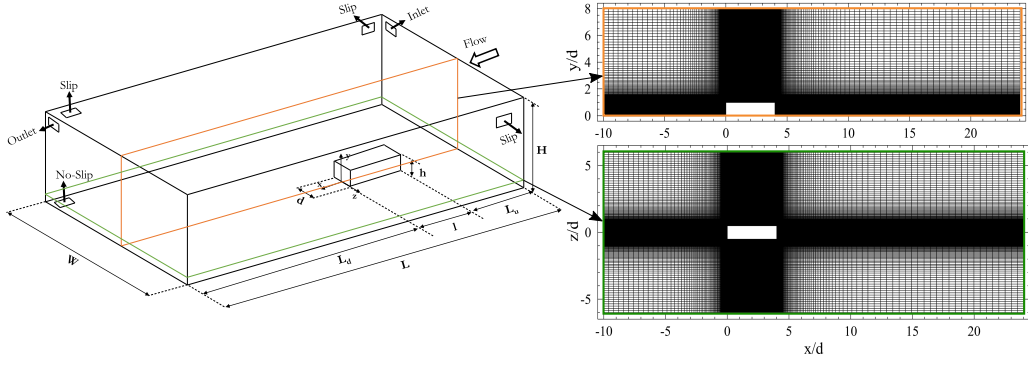


Figure 1. Computational domain (Not to scale) and spatial grid distribution for the wall mounted thin prism of $DR = 1$, presented in Top view at $y/d = 0.5$ (top) and side view at $z/d = 0$ (bottom).

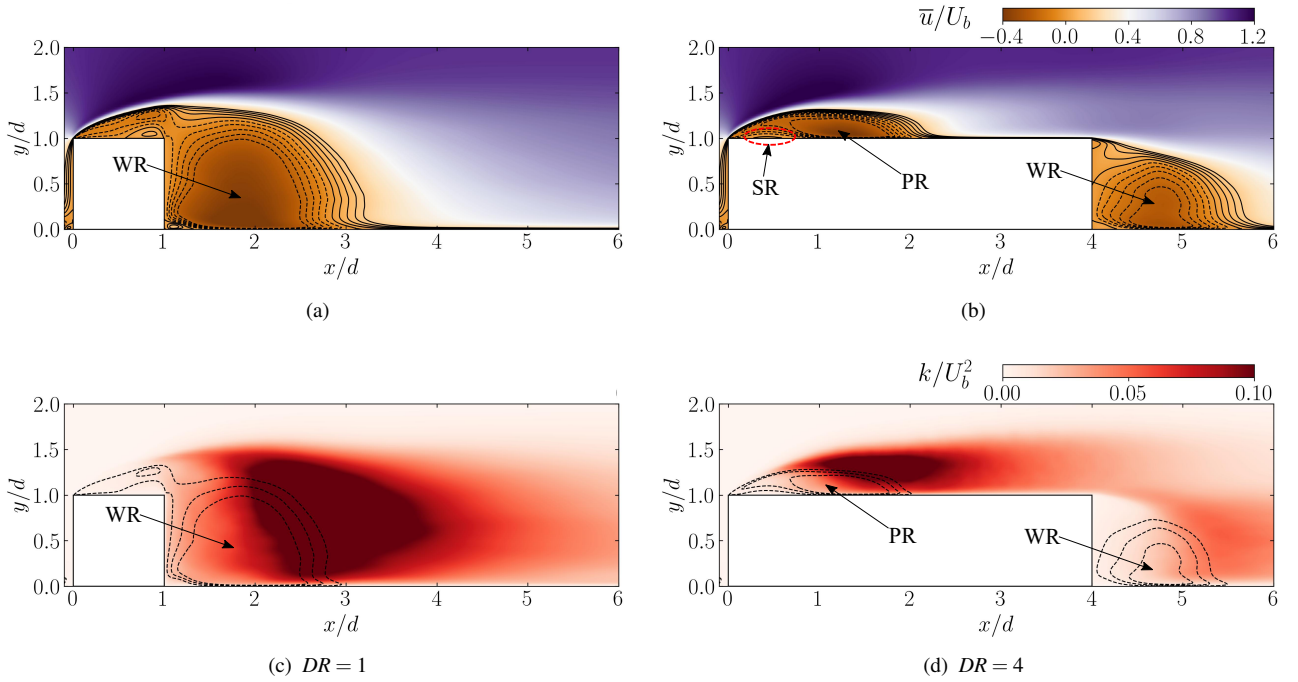


Figure 2. Mean streamwise velocity (\bar{u}) and turbulent kinetic energy (k) contours overlaid with mean velocity streamlines for (a, c) $DR = 1$ and (b, d) $DR = 4$ prisms.

A non-homogeneous structured grid consisting of 25×10^6 and 40×10^6 elements was developed for this study. Domain and grid for the case of $DR = 4$ are presented in Figure 1. The inlet boundary conditions were set to uniform flow ($u = U_b, v = w = 0$), with an outflow boundary condition ($\partial u / \partial n = \partial p / \partial n = 0$) applied at the outlet. Ceiling and lateral boundaries were modeled as free-slip, while no-slip wall condition was imposed on the ground and the prism. This computational setup closely resembled that of Goswami & Hemmati (2022). Second-order implicit Backward Euler numerical schemes were used for temporal discretization, and the diffusive and convective fluxes were approximated using central difference schemes. The discretized equations were then solved using a Pressure Implicit with Splitting Operator (PISO)-based algorithm (Goswami & Hemmati, 2022). Time-marching simulations were performed by adjusting the temporal grid to maintain a maximum Courant-Friedrichs-Levy number (CFL) below 0.8. All simulations continued for 150 vortex shedding cycles, with the last 80 cycles used for post-processing.

Results & Discussion

We begin by reporting the main features of the mean flow. As shown in Figure 2a and 2b, the streamlines highlight the presence of a separation at the leading edge, which in case of $DR = 1$ prolongs into the wake and reattaches at $x/d \approx 2.12$ for $DR = 4$. A large scale recirculation region is present on the top surface of $DR = 4$, hereby referred to as the primary recirculation (PR) region. A second recirculation bubble is present below the primary recirculation region, noted as secondary recirculation (SR) zone. Indeed, the reverse flow induced in the near-wall region of the primary recirculation forms a boundary-layer moving upstream, resulting in the secondary recirculation region. Following the trailing-edge separation of the flow, a tertiary recirculation region is formed, referred to as the wake recirculation (WR) region. For the short prism, the absence of PR and SR is attributed to a lack of flow reattachment on the prism surfaces. As such, only WR is noted due to the leading-edge shear-layer shedding directly into the wake. Contours of turbulence kinetic energy ($k = (u'_i u'_i) / 2$) are presented in Figure 2c and 2d. Initially, both prisms highlight an almost laminar state of the leading-edge shear-layer. Insta-

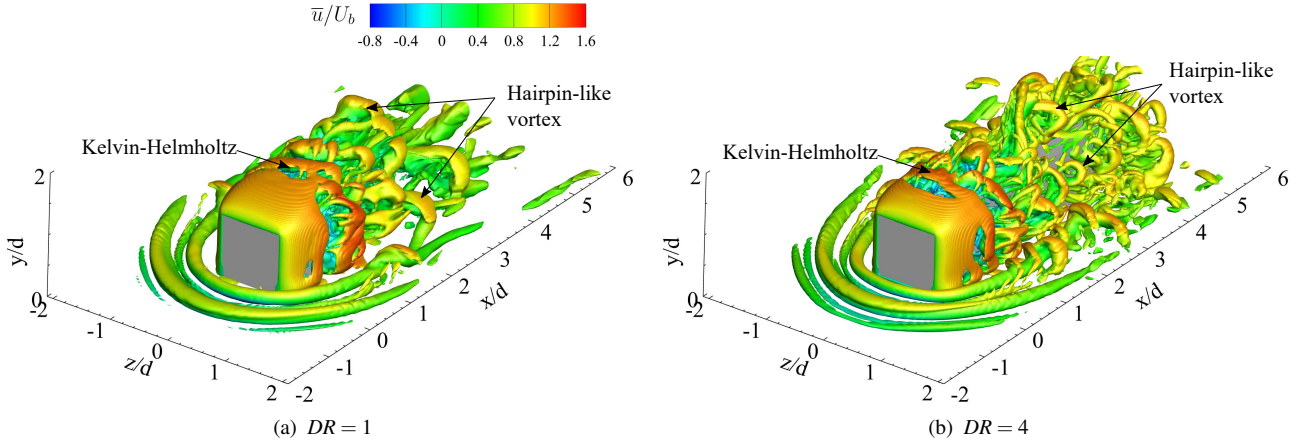


Figure 3. Instantaneous vortex structures overlaid with axial velocity (u) contours for (a) $DR = 1$ and (b) $DR = 4$ prisms identified using Q -criterion ($Q^* = 1 \times 10^{-4}$).

bilities associated with the leading-edge shear-layer amplify the intensity of fluctuating velocities, initiating the transition-to-turbulence (Wang & Zhou, 2009). These regions of intense fluctuations result in high turbulence intensity (u'_t) and thus maximizing k . For the larger prisms the maximum k occurs on the prism top surface, while the shorter prisms experience the maximum k in the wake. The region of maximum k occurs in the primary vortex shedding region.

Qualitative illustrations of the instantaneous vortex structures for $DR = 1$ and 4 are presented in Figure 3. Following the leading-edge separation, shear-layer undergoes distinct stages of growth and primary instability formation (Moore *et al.*, 2019). This triggers the formation of Kelvin-Helmholtz instability (KHI) of the shear-layer for $DR = 4$, as evident by the finite spanwise vortex rollers forming near the leading edge. Such rollers are absent for $DR = 1$, underscoring the influence of depth-ratio in the generation of these instabilities. Further, leading edge shear-layer sheds directly into the wake for the case of $DR = 1$, while the flow reattaches on the surfaces of the larger prism. The later prism shows a prominent span-wise vortex shedding with hairpin-like vortices appearing over the prism surfaces. However vortex shedding is suppressed by interactions between the separating shear-layer and the wake in WR for shorter prism. These observations along with the formation of KHI rollers and their interaction with surfaces of the prism are a precursor to the transition-to-turbulence in the wake of wall-mounted prisms.

Previously, Rastan *et al.* (2021) showed that increasing depth-ratio for a large AR prism resulted in decreased vortex shedding due to diminished interactions between the separating shear-layer and the wake. This effect correlates with the strengthening of the downwash flow. These results are consistent with the wake observed behind low aspect-ratio prisms (Goswami & Hemmati, 2022). In fact, increasing DR suppresses the wake unsteadiness. The present study portrays a contrary view, where the wake unsteadiness is enhanced with increasing depth-ratio. While the wake dynamics change significantly with depth-ratio and aspect-ratio, the current results suggest that Reynolds number plays a dominant role in the transition process. At moderate Reynolds numbers, the shear-layer flapping motion is stronger, which interact with the prism surfaces and elevate the flow momentum in this region due to large depth-ratio. This further enhances the interactions between KHI and the wake coherent structures, leading to the wake transition. Evidence of this mechanism is discussed fur-

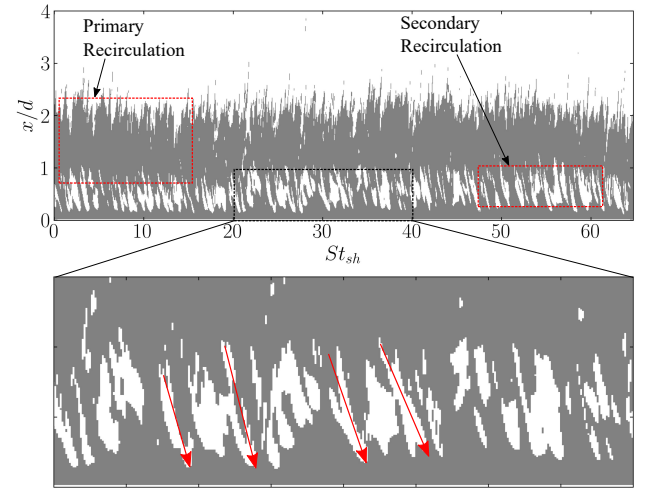


Figure 4. Space-time plot of the instantaneous wall shear-stress (τ_w) along the top surface of the prism with $DR = 4$ at $z/d = 0$. $\tau_w > 0$ (White) represents the region of forward flow, while $\tau_w < 0$ (Gray) represents the region of reverse flow.

ther in this article by first presenting the shear-layer flapping motion, followed by the wake frequency signatures, and enhanced interactions using the Poisson equation. Finally, the triadic interactions are quantified using bi-spectral mode decomposition (BMD) to further understand the transition phenomenon. Here we look at the interactions between KHI and the large-scale vortex shedding.

The shear-layer flapping motion is quantitatively analyzed using the wall shear-stress ($\tau_w = \mu \partial u / \partial x$) along the top surface of the long prism, as depicted in Figure 4. Temporal variations between the mean reattachment point are recognized by the border between the reverse flow ($\tau_w < 0$) and forward flow ($\tau_w > 0$) regions. Previous studies (Lander *et al.*, 2018) suggest two main mechanisms that control the flow unsteadiness around sharp edged prisms: vorticity-roll-up and shear-layer flapping. For long prisms, the shear-layer roll-up near the leading-edge intermittently forces the newly formed vortices towards the prism surfaces, resulting in a flapping motion (Moore *et al.*, 2019). This induces oscillations of the primary recirculation bubble (PR). As presented in Figure 4, mean reattachment point at $z/d = 0$ for the large depth-ratio

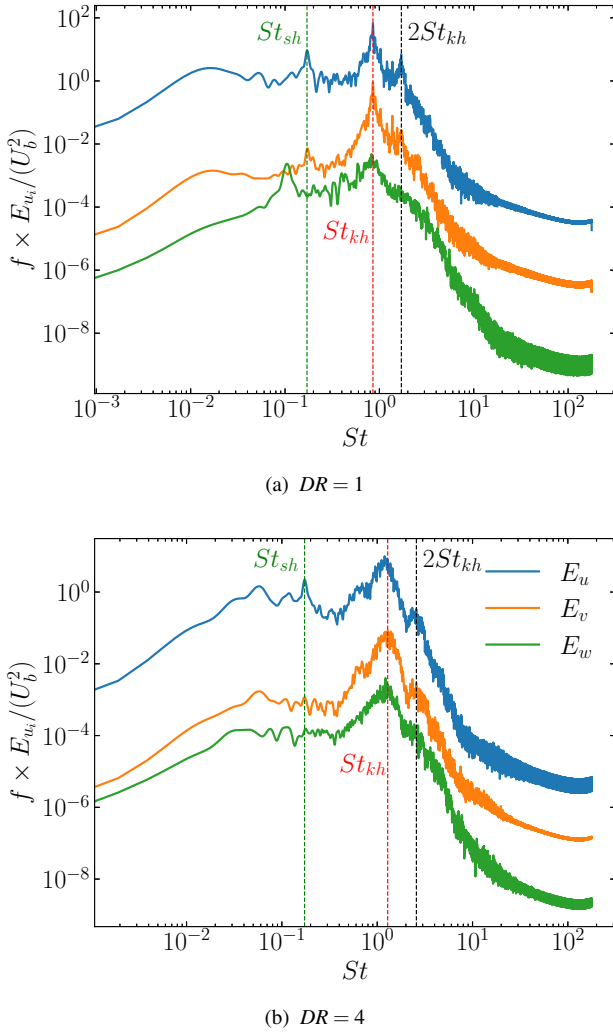


Figure 5. Pre-multiplied power spectral density of streamwise (E_u), normal (E_v) and spanwise (E_w) velocity fluctuations near the leading-edge at $(0.5, 1.3, 0)$ for (a) $DR = 1$ and (b) $DR = 4$.

prism follows an oscillatory pattern. The primary recirculation region is observed to oscillate between $x/d \approx 1.2$ and ≈ 2.1 . Further, secondary recirculation bubble also appears to oscillate, albeit in the opposite direction. With time, the secondary recirculation region moves further upstream, while the primary recirculation bubble moves downstream. This behavior may be linked to the mechanism of shear-layer flapping, though it remains out of scope of this study.

Further, the flow periodicity is investigated by using the pre-multiplied power spectral density of the streamwise (E_u), normal (E_v) and spanwise (E_w) velocity fluctuations near the leading-edge at $(0.5, 1.3, 0)$ in Figure 5. Multiple peaks are noted in the power spectrum of both cases, with the one at St_{kh} appearing to be dominant. This frequency is associated with KHI of the leading-edge shear-layer. Moreover a harmonic of KHI is observed at $2St_{kh}$. Another frequency centered at St_{sh} is also observed, mainly attributed to the Kármán-like vortex shedding. At $DR = 1$, St_{sh} and St_{kh} are 0.170 and 0.855, respectively. For $DR = 4$, they are 0.173 and 1.290, respectively. With increasing depth-ratio from 1 to 4, a meager increase in St_{sh} is noted, while St_{kh} and $2St_{kh}$ are significantly enhanced. In other words, the depth-ratio enhances KHI of the leading-edge shear-layer, and further explains the strong span-wise vortex shedding (observed in Figure 3b). Finally, a

sub-harmonic spanwise frequency is noted, which is attributed to alternate shedding of the secondary vortex structures in the wake (Goswami & Hemmati, 2022).

Shear-layer flapping motion is correlated with the vortex-pairing mechanism in sharp-edged prisms (Ma *et al.*, 2023). Following the flow separation at the leading-edge, the shear-layer rolls-up due to KHI, and the newly formed vortices are intermittently forced towards the prism surfaces and convect downstream (flapping mechanism). These vortices pair with other vortices in the wake, growing into large-scale structures, such as hairpin-like vortices (vortex-pairing mechanism). The large scale vortex shedding away from the leading edge is associated with large scale momentum transport. The vortex-pairing and interactions of KHI with the large-scale vortices are quantified using the correlation, $St_{kh}/St_{sh} = 0.18Re^{0.6}$ (Lander *et al.*, 2018). The interactions are a function of Reynolds number and ideally this ratio should be 18 for $Re = 2.5 \times 10^3$. The results in Figure 5 indicate that this ratio is ~ 5.0 and ~ 7.5 for $DR = 1$ and 4, respectively. This suggests that the interactions between KHI and the large-scale structures depend on the depth-ratio, and the interactions are suppressed compared to infinite span prisms due to the three-dimensional effects of the wall-mounted prism flow.

Interactions between KHI and large-scale vortex shedding can be further quantified by analyzing the Poisson equation:

$$\nabla^2 p = -\rho \left(2 \frac{\partial \overline{u_i}}{\partial x_j} \frac{\partial u'_j}{\partial x_i} + \frac{\partial^2}{\partial x_i \partial x_j} (u'_i u'_j - \overline{u'_i u'_j}) \right).$$

Here the right-hand side can be decomposed into two terms: turbulence-mean-shear interaction (TMI) and turbulence-turbulence interaction (TTI). TMI accounts for the rapid changes in mean flow due to fluctuating fields, while TTI is associated with non-linear interactions of turbulent structures. These two terms are considered the primary sources of pressure fluctuations in the flow (Ma *et al.*, 2023).

Figure 6 presents the profiles of maximum values of TMI and TTI terms of the Poisson equation for $DR = 1$ and 4 at $z/d = 0$ (Blue) and $y/d = 0.5$ (red). Figure 6a reveals heightened turbulence-mean-shear interactions closer to the leading edge, where separated shear-layers are created, for both prisms. Following the abrupt shear-layer separation at the leading-edge, vorticity associated with the shear-layer alter the mean flow in this region, resulting in enhanced momentum. This explains the high values of TMI near the leading-edge. Initially, TMI_{\max} for both prisms remains large, though it subsides quickly for $DR = 1$. Due to a lack of flow reattachment in $DR = 1$, TMI_{\max} for top shear-layer reduces till $x/l \approx 0.5$, followed by a gradual increase due flow interaction with the upwash flow at the trailing edge (Goswami & Hemmati, 2023). TMI for $DR = 4$ remains large in $0.1 \leq x/l \leq 0.3$, indicating region of elevated mean-flow modulations by KHI. For both cases, TMI_{\max} on side surfaces is significantly suppressed compared to the top, indicating that the top surface shear-layer plays a dominant role in driving the downstream flow. Finally, TMI points to the origins of mean flow modulations, which are associated with the shear-layer flapping motion. Thus, enhanced TMI near the leading-edge for $DR = 4$ show where the shear-layer flapping motion is most pronounced.

The TTI term, presented in Figure 6b, highlights the interactions between different flow structures (Ma *et al.*, 2023). While TMI is concentrated near the leading-edge, TTI is more distributed across the top and side surfaces of both prisms. The distribution is likely due to the enhanced flow momentum

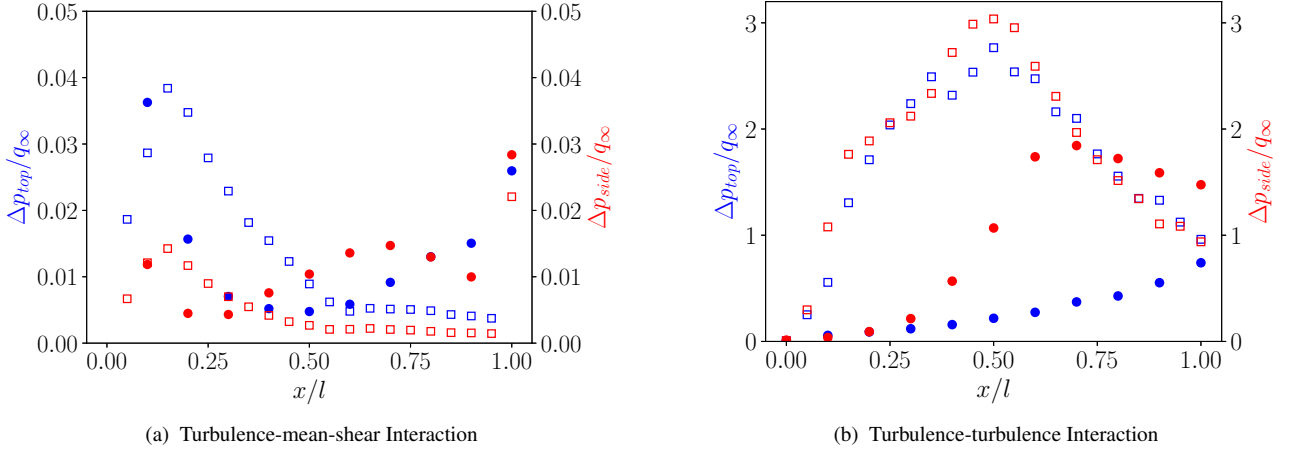


Figure 6. Profiles of maximum values of root-mean-squared (a) turbulence-mean-shear interaction (TMI_{\max}) and (b) turbulence-turbulence interaction (TTI_{\max}) terms of the pressure Poisson's equation for $DR = 1$ and 4 prisms at $z/d = 0$ (Blue) and $y/d = 0.5$ (red). The axial distances are normalized using prism length (l). \circ represents $DR = 1$; \square represents $DR = 4$.

(velocity fluctuations) produced by the mean flow alterations by TMI gradually affecting the surrounding flow field. For $DR = 1$, TTI_{\max} is elevated closer to the trailing-edge, which is attributed to the direct shedding of the leading-edge shear-layer into the wake. This enhances the interactions and vortex mixing in the wake region (WR) (Goswami & Hemmati, 2023). For $DR = 4$, elevated TTI_{\max} occurs close to location of the flow reattachment on the prism surfaces ($\bar{x}_R/l \approx 0.53$). This region is associated with the breakdown of KHI rollers into hairpin-like vortices, which are then convected downstream. The interactions between KHI rollers and large-scale vortex shedding are most pronounced in this region, leading to an increased turbulence intensity and mixing (results not presented here for brevity). These processes enhance the flow momentum due to an influx of energy by the mean flow modulation (TMI). As such, increased momentum results in enhancement of vortex shedding and wake transition. Further, these interactions are driven by the flow geometry, since such a mechanism is absent for the short prism, where the TTI_{\max} steadily rises up to the trailing-edge. Finally, TTI_{\max} are comparable for the top and side surface shear-layers of both prisms, indicating a balance of energy transfer between the two surfaces (not presented for brevity).

Finally, triadic interactions form the basis of the mechanism of energy transfer in the flow and the wake transition phenomenon (Craik, 1971). Frequency triad, described by the interactions between two flow structures at frequencies St_i and St_j , results in a third frequency of St_{i+j} such that $St_i \pm St_j \pm St_{i+j} = 0$. These interactions are quantified using bi-spectral mode decomposition (BMD) analysis, proposed by Schmidt (2020). Figure 7 shows the magnitude of mode bi-spectrum for $DR = 4$ in the sum and difference regions. Their interactions with large-scale vortex shedding frequency (St_{sh}) are noted in Figure 7, along with the sum interaction of St_{kh} with St_{sh} and the fundamental mode of St_{sh} . Magnitude of the spectrum is large of the large-scale frequencies, while it reduces significantly for St_{kh} . Further, the sum interaction of St_{sh} corresponds to the global maximum of mode bi-spectrum, consistent with the separated flow in Schmidt (2020).

The interactions of KHI with the mean flow, triad $(0, St_{kh}, St_{kh})$, and large-scale vortex shedding, triad $(St_{sh}, St_{kh}, St_{kh} + St_{sh})$, are presented in Figure 8. For both cases, the interactions are most pronounced near the

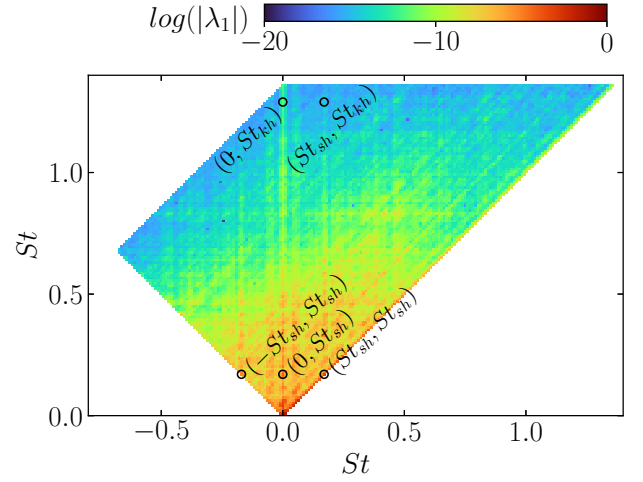


Figure 7. Magnitude mode bi-spectrum for $DR = 4$, using $N_{fft} = 2^8$, in the sum and difference regions.

leading-edge and through-out the upper surface of the prism up to $x/d \approx 2$, where the flow reattaches to the surface. Interactions of KHI with the mean flow is dominant outside the primary recirculation region, with the maximum value occurring at $x/d \approx 0.8$. This is consistent with the location of maximum turbulence-mean-shear interactions in Figure 6a. This interaction is associated with the mean-flow modulation by KHI due to shear-layer flapping motion. A slightly elevated interaction at the trailing edge also corresponds to the trailing-edge shear-layer interacting with the flow downstream. The interactions of KHI with the large-scale vortex shedding are distributed across the prism surface. Near the center of the primary recirculation region, these interactions enhance due to the flow impingement of prism surfaces as a result of shear-layer flapping. This region of elevated interactions is consistent with the region of maximum turbulence-turbulence interactions in Figure 6b. These results confirm that the flow modulations at the leading-edge due to KHI are convected downstream and interact with the large-scale vortex shedding, enhancing the flow momentum. Due to the interactions and vortex breakdown, the flow momentum reduces further till

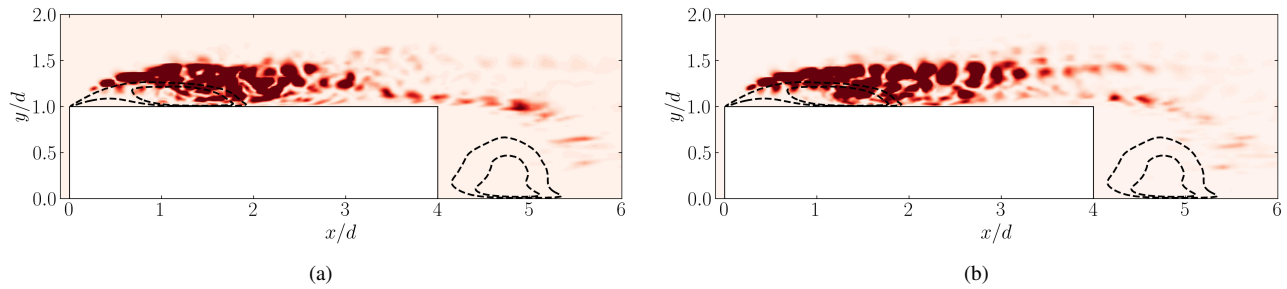


Figure 8. BMD interaction map for $DR = 4$ prism, showing the interactions between (a) Kelvin-Helmholtz instability and mean flow and (b) Kelvin-Helmholtz instability and large-scale vortex shedding.

the trailing-edge. While not showed here for $DR = 1$, such interactions remain absent, underscoring the influence of depth-ratio in the wake transition phenomenon.

Conclusions

This study presents a numerical investigation of the wake transition phenomenon behind wall-mounted prisms. Results were presented at Reynolds number of 2.5×10^3 for prisms with aspect-ratio of 1 and depth-ratios of 1 and 4. The wake unsteadiness is enhanced with increasing depth-ratio. Kelvin-Helmholtz instability is noted for the longer prisms, forming finite spanwise vortex rollers. Enhanced wake unsteadiness is attributed to the interactions between Kelvin-Helmholtz instability and large-scale vortex shedding, driven by the shear-layer flapping motion in the large depth-ratio prism. Evidence of shear-layer flapping is provided by analyzing the space-time wall shear-stress contours, showing an oscillating recirculating region. Interactions between Kelvin-Helmholtz instability and large-scale vortex shedding are quantified using the Poisson equation and bi-spectral decomposition. Turbulence-mean-shear interaction (TMI) term of Poisson's equation is elevated near leading-edge, while the turbulence-turbulence interaction (TTI) term is distributed across the prism surfaces. Elevated TMI near the leading-edge points to the mean flow manipulations due to shear-layer flapping, while the enhanced TTI on the prism surfaces indicates the interactions between the Kelvin-Helmholtz instability and large-scale vortex shedding. Elevated TMI shows that the leading-edge flow manipulations provide energy which is then transferred to the large-scale vortex shedding, enhancing the flow momentum. Increased momentum in the wake enhances the vortex shedding, which is a precursor to turbulence transition. Finally, the bi-spectral mode decomposition analysis provides evidence of interactions between the Kelvin-Helmholtz instability and large-scale vortex shedding, further confirming the transition process. The study underscores the role of depth-ratio in the transition-to-turbulence phenomenon at moderate Reynolds numbers.

REFERENCES

Craik, Alex DD 1971 Non-linear resonant instability in boundary layers. *Journal of Fluid Mechanics* **50** (2), 393–413.

- Durbin, Paul A & Reif, BA Pettersson 2011 *Statistical theory and modeling for turbulent flows*. John Wiley & Sons.
- Goswami, Shubham & Hemmati, Arman 2022 Mechanisms of wake asymmetry and secondary structures behind low aspect-ratio wall-mounted prisms. *Journal of Fluid Mechanics* **950**, A31.
- Goswami, Shubham & Hemmati, Arman 2023 Mean wake evolution behind low aspect-ratio wall-mounted finite prisms. *International Journal of Heat and Fluid Flow* **104**, 109237.
- Lander, DC, Moore, DM, Letchford, CW & Amitay, M 2018 Scaling of square-prism shear layers. *Journal of Fluid Mechanics* **849**, 1096–1119.
- Ma, Chung-Hao, Awasthi, Manuj, Moreau, Danielle & Doolan, Con 2023 Aeroacoustics of turbulent flow over a forward-backward facing step. *Journal of Sound and Vibration* **563**, 117840.
- Moore, DM, Letchford, CW & Amitay, M 2019 Energetic scales in a bluff body shear layer. *Journal of Fluid Mechanics* **875**, 543–575.
- Rastan, MR, Shahbazi, H, Sohankar, A, Alam, Md Mahub & Zhou, Yu 2021 The wake of a wall-mounted rectangular cylinder: Cross-sectional aspect ratio effect. *Journal of Wind Engineering and Industrial Aerodynamics* **213**, 104615.
- Saha, Arun K 2013 Unsteady flow past a finite square cylinder mounted on a wall at low Reynolds number. *Computers & Fluids* **88**, 599–615.
- Schmidt, Oliver T 2020 Bispectral mode decomposition of nonlinear flows. *Nonlinear dynamics* **102** (4), 2479–2501.
- Wang, HF & Zhou, Yu 2009 The finite-length square cylinder near wake. *Journal of Fluid Mechanics* **638**, 453–490.
- Zargar, Arash, Tarokh, Ali & Hemmati, Arman 2022 The unsteady wake transition behind a wall-mounted large-depth-ratio prism. *Journal of Fluid Mechanics* **952**, A12.
- Zdravkovich, Momchilo M 1997 *Flow around circular cylinders: Volume 2: Applications*, vol. 2. Oxford university press.